Nano Research 2014, 7(4): 553–560
DOI 10.1007/s12274-014-0423-1
Research Article
ISSN 1998-0124
CN 11-5974/O4

Heating graphene to incandescence and the measurement of its work function by the thermionic emission method

Feng Zhu[1,2,§], Xiaoyang Lin[1,2,§], Peng Liu[1,2] (✉), Kaili Jiang[1,2] (✉), Yang Wei[1,2], Yang Wu[1,2], Jiaping Wang[1,2], and Shoushan Fan[1,2]

[1] *State Key Laboratory of Low-Dimensional Quantum Physics, Department of Physics and Tsinghua–Foxconn Nanotechnology Research Center, Tsinghua University, Beijing 100084, China*
[2] *Collaborative Innovation Center of Quantum Matter, Beijing 100084, China*
[§] *The first two authors contributed equally to this work.*

Received: 3 November 2013
Revised: 14 January 2014
Accepted: 20 January 2014

KEYWORDS
graphene,
carbon nanotube,
thermionic emission,
work function

ABSTRACT

The work function (WF) of graphene is an essential parameter in graphene electronics. We have derived the WF of graphene by the thermionic emission method. Chemical vapor deposition (CVD)-grown single-layered polycrystalline graphene on copper foil is transferred to a cross-stacked carbon nanotube (CNT) film drawn from a super-aligned multiwalled CNT array. By decreasing the pore size of the CNT film, the as-prepared CNT-graphene film (CGF) can be Joule heated to a temperature as high as 1,800 K in vacuum without obvious destruction in the graphene structure. By studying the thermionic emission, we derive the WF of graphene, ranging from 4.7 to 4.8 eV with the average value being 4.74 eV. Because the substrate influence can be minimized by virtue of the porous nature of the CNT film and the influence of adsorbents can be excluded due to the high temperature during the thermionic emission, the measured WF of graphene can be regarded as intrinsic.

1 Introduction

As a one-atom thick two-dimensional film of carbon, graphene has become extremely attractive owing to its high carrier mobility [1, 2], superior thermal conductivity [3–5], and interesting physics [6, 7]. Researchers have also proposed many applications for this monolayer carbon film, such as field effect tunneling transistors [8, 9], optical modulators [10], transparent electrodes for touch panels [11] and organic solar cells [12]. In all such graphene electronics, the work function (WF) is a fundamental parameter that will influence the performance of the devices.

In previous work, several methods, including scanning Kelvin probe microscopy (SKPM) [13–15], scanning tunneling microscope (STM) [16], low-energy

Address correspondence to Peng Liu, pengliu@mail.tsinghua.edu.cn; Kaili Jiang, Jiangkl@mail.tsinghua.edu.cn

electron microscope (LEEM) [17], and angle-resolved ultraviolet photoelectron spectroscopy (ARUPS) [18–20], have been used to determine the WF of graphene. However, the reported values vary from 3.7 to 5.2 eV. As has been pointed out in literatures [17, 20–23], two factors will definitely influence the measurement of WF. The first one is the interaction between graphene and the substrate. Even for multi-layered graphene, the electronic structure of the graphene changes with the layer number as shown by the angle resolved photoelectron spectroscopy (ARPES) results [22–24]. Therefore, it is best to suspend a single-layered graphene to get its intrinsic WF. The other factor is the absorbents, which will influence the accuracy of the WF measurement [21, 25]. A method that can eliminate the effect of adsorbents is still desired.

The first requirement is difficult to satisfy because of the fragility of single-layered graphene. Thus most of the studies about graphene still focus on samples on a substrate like a silicon wafer. We have recently demonstrated a carbon nanotube (CNT)–graphene hybrid film (CGF) [26], which utilizes a super-aligned CNT film as a porous support for graphene, can give large area single-layered graphene suspended on the porous CNT network. Due to the porous nature of the CNT network support, most of the graphene can be regarded as being suspended. As a result, the substrate influence can be minimized in such a structure. The second requirement can be fulfilled using the thermionic emission method, in which the adsorbents can be removed automatically due to the high temperature during emission. Because CNT films can be heated to incandescence and their WF has already been studied with the thermionic emission method [27], the CGF will be a suitable choice for thermionic emission experiments.

In this work, the WF of graphene was measured with the CGF sample by the thermionic emission method. It is found that by decreasing the pore size of the CNT network support, the graphene can keep its structural integrity at high temperatures. Scanning electron microscopy (SEM) and Raman spectroscopy indicate that the graphene structure in CGF has no significant difference before and after annealing. With a symmetric anode structure, the WF of graphene and the CNT film can be measured separately at the same time. The WF of graphene ranges from 4.7 to 4.8 eV, with the average value being 4.74 eV. The WF of graphene measured in this work is regarded as being close to the intrinsic value.

2 Experimental

The graphene we used was synthesized by chemical vapor deposition (CVD) on polycrystalline copper foil [28] with a macroscopic size on the order of several square centimeters. Figure 1(a) shows a SEM image of the as-grown graphene on copper foil. The Raman spectrum excited by a 514 nm laser is shown in Fig. 1(b), in which the 2D peak is roughly four times more intense than the G peak, verifying that the surface is covered predominately by single-layered graphene [29]. The negligible intensity of the defect-induced D peak shows the good quality of the sample.

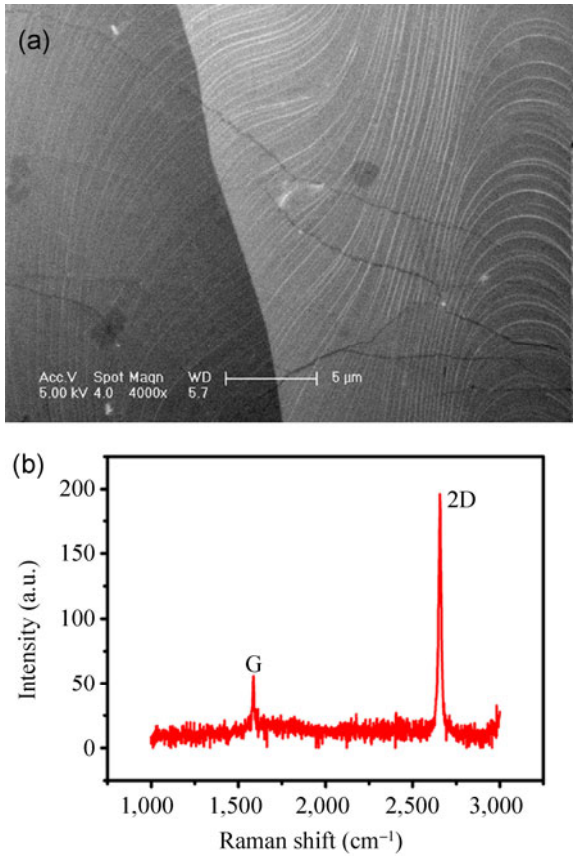

Figure 1 (a) SEM image of the CVD-grown polycrystalline graphene on copper foil. (b) Raman spectra excited by 514 nm laser of the as-grown graphene on copper foil.

Continuous CNT thin films are directly drawn out from super-aligned multiwalled CNT array, as has been shown in the previous several fascinating applications [30, 31]. The CNT film is ultra-thin, transparent, conductive and flexible. It is also very stable under Joule heating to incandescence and therefore is applicable to thermionic emission experiments [27, 32]. Furthermore, the CNT is composed of the same atoms and lattice structure as graphene. It will not form strong dipole interactions with graphene, and together with its porous nature, should have a minimal influence on the graphene WF compared with other substrates [20]. The graphene is transferred to the CNT film and form a hybrid CNT-graphene film (CGF). The integrity of graphene at the scale of several square centimeters can be sustained. In addition, the transfer process does not introduce the polymers such as polymethylmethacrylate (PMMA) or polydimethylsiloxane (PDMS) which are commonly used in conventional processes [33, 34], resulting in the graphene surface being very clean without polymer contamination. Figures 2(a) and 2(b) show the SEM images of the CGF with two-layered CNT film from the graphene and CNT side separately. It can be found that graphene covers one side of the CNT film (Fig. 2(a)), causing the CNT under to be dim(Fig. 2(a)). In figure 2(b), the graphene can also be seen through the pore on CNT network.

As we have mentioned above, to study the thermionic emission of the graphene, the sample must be able to withstand the high temperature during the emission. It is found that the number of CNT layers is a key factor in ensuring the graphene retains its structural integrity. Figures 2(c) shows the CGF with two-layered CNT films after being heated to incandescence. The graphene breaks down into small pieces left on the skeleton of CNT network. It is found that the graphene pieces on the small pores can stay there regardless of the annealing time. The reason for the breakdown of graphene probably lies in the discrepancy between the coefficient of thermal expansion (CTE) of the CNT film and graphene. The CTE of graphene is reported to be much smaller than that of CNT [35–39], and actually it is negative at room temperature [36, 38, 39]. Thus the graphene will suffer a tension force during the heating process, causing the appearance of some cracks where defects and grain boundaries exist (Fig. 2(f)). These cracks will lead to the breakdown of the graphene on large pores in the two-layered CNT film (Fig. 2(b)), while the extension of the cracks can be confined on the small pores. [26]. When we adopted an eight-layered CNT film as the substrate which has much smaller pore

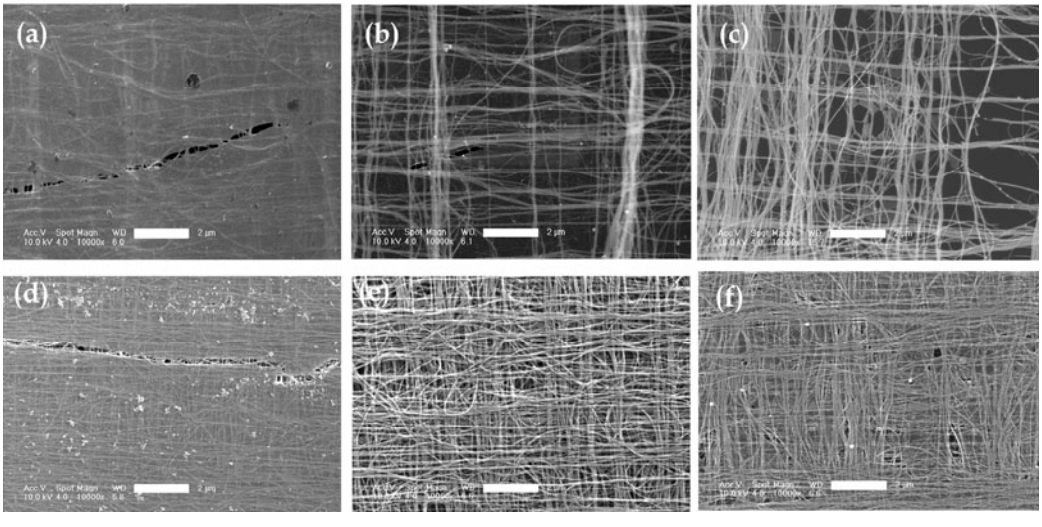

Figure 2 The SEM images of CGF: (a) graphene on two-layered CNT film observed from the graphene side; (b) graphene on two-layered CNT film observed from the CNT side; (c) graphene on two-layered CNT film observed from the graphene side after annealing at a temperature of 1,800 K; (d) graphene on eight-layered CNT film observed from the graphene side; (e) graphene on eight-layered CNT film observed from the CNT side; (f) graphene on eight-layered CNT film observed from the graphene side after annealing at 1,800 K for 4 hours.

size (Figs. 2(d)–2(f)), it was found that the graphene can retain its structure integrity even after high temperature annealing for four hours in spite of the appearance of some small cracks (Fig. 2(f)).

When the CGF being heated to incandescence, obvious thermionic emission current can be detected. Figure 3(a) shows the image of CGF being heated to incandescence. The red curve in Fig. 3(b) shows the current–voltage (*I*–*V*) curve when we used a single anode to collect the emission current from the graphene side. There are some steps (the arrow) on the curve and the current seems to be unsaturated even when the voltage is as high as 400 V. This unsaturation can be attributed to the electrons emitted from the CNT side, which will be collected from the graphene side at high anode voltages. It will influence the WF measurement. Therefore, a two-sided symmetric anode structure was adopted to collect the thermionic emission current from both sides separately. The arrangement is schematically illustrated in Fig. 3(c). Two pieces of indium tin oxide (ITO) glass are symmetrically placed as anodes to collect the thermionic emitted electrons. The CGF is Joule heated across two copper electrodes, which are fixed with a spacing of 3 mm. Figure 3(d) shows the corresponding schematic electric circuit. The same voltage is applied to both ITO anodes synchronously. The blue line in Fig. 3(b) is the *I*–*V* curve of the CGF collected from the graphene side using the symmetric anode structure, showing a long accelerating field region, fitted well with the Schottky effect [40, 41]. To prove that the anode on the graphene side only collects the emission current from graphene, several samples of pure CNT films and CGFs of the same size were tested with the symmetric anode structure. As shown in Fig. 4, the thermionic emission currents collected from the CNT side of CGF and those of pure CNT films are all almost the same, with the difference being no more than 5%. This demonstrates the reliability of the symmetric anode structure. Meanwhile, as Fig. 4 shows, the emission current collected from the graphene side of CGF is about 25%–30% larger than that from the CNT side. The reason for this may lie in the difference in emission areas between the CNT films and graphene. More discussion of this can be found in the Electronic Supplementary Material (ESM).

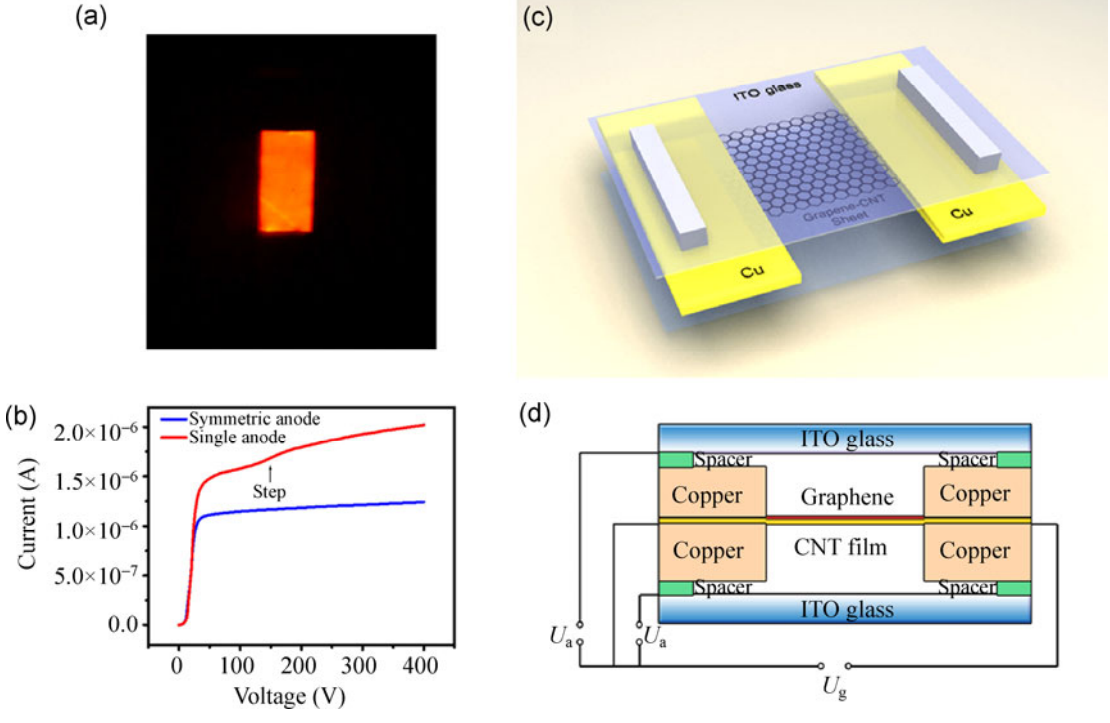

Figure 3 (a) Optical image of the heated CGF. (b) *I*–*V* curves of the thermionic emission of the CGF collected from the graphene side using a single anode (red line) and a symmetric anode (blue line). (c) Three-dimensional illustration of the testing structure. (d) Schematic electronic circuit of the experiment.

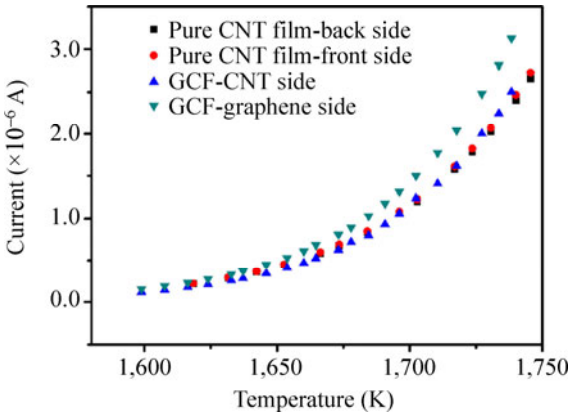

Figure 4 Thermionic emission current collected from CNT side of the CGF (blue triangles); graphene side of the CGF (green inverted triangles); front (red circles) and back side (black squares) of pure CNT films at different temperatures. The anode voltage is 500 V for all samples.

3 Results and discussion

The temperature was obtained by fitting the optical spectra in the visible light range with Plank's law of black bodies. According to the Schottky effect [40, 41], the zero-field current I_0 at different temperatures can be derived from the $\ln(I_a)$ vs. $U^{1/2}$ curves, where I_a is the current collected by the anode and U is the anode voltage. Then, according to Richardson's formula [41], the WF can be derived from I_0 and the temperature. The theory and the detailed method are discussed in the ESM.

To get an obvious thermionic emission current, the measurement temperature was set from 1,500 to 1,800 K. We first measured the WF of a pure CNT film with the symmetric anode structure. Five samples were measured. The WF of the CNT film is in the range 4.77 eV ± 0.07 eV. Note that the CNT films in this experiment are shrunk and have no protruding tips with lower WF, and the result is in good accordance with previous measurements in the literature [27, 32, 42]. The difference in WF between the two sides of the CNT film ranges from 0.03 to 0.15 eV. Therefore, if the WF difference between the two sides is less than 0.15 eV, it cannot be distinguished in our experiment.

Figure 5(a) shows the typical $\ln(I_a)$ vs. $U^{1/2}$ curve and the $\ln(I_0/T^2)$ vs. $1/T$ plots for the graphene samples we have measured. The WF value is derived from the slope of the linear fitting curve of the dots in Fig. 5(b). The good linearity of the plot indicates the accuracy of the measurements. The WF of graphene lies in the range of 4.7 to 4.8 eV, with an average value of 4.74 eV ± 0.04 eV (Fig. 6(a)). The error bar of each data point in Fig. 6(a) is the Type A uncertainty determined by the standard deviation of the linear fitting of the $\ln(I_0/T^2)$ vs. $1/T$ curve. The uncertainty of the average value is obtained by the law of propagation of uncertainty [43]. This uncertainty represents the random error of our experiment. The frequency distribution of the WF of graphene is presented in a histogram in Fig. 6(b), in which the most probable result is exactly the average value, indicating good statistical consistency of our experimental results. Meanwhile, the WF derived from the CNT side is 4.78 eV ± 0.05 eV. This is in good accordance with the measured value of pure CNT films, verifying the reliability of the measurements.

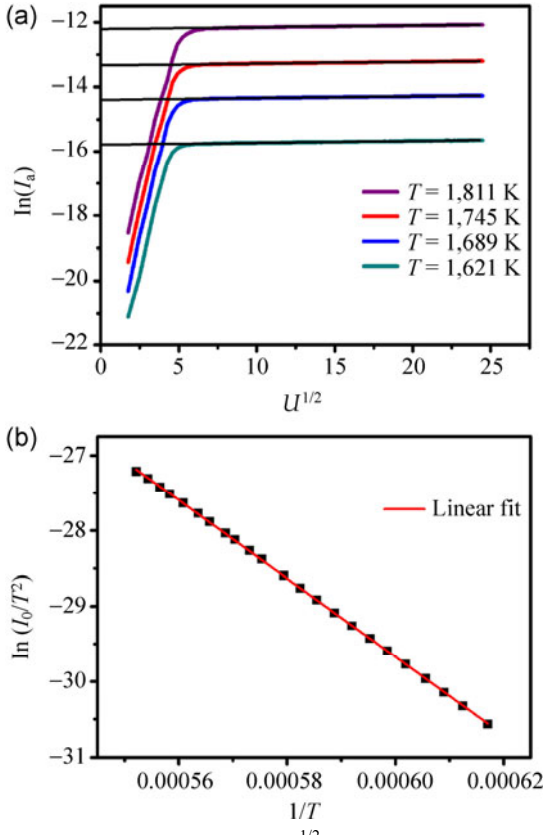

Figure 5 (a) Typical $\ln(I_a)$ vs. $U^{1/2}$ curve for the graphene on CNT film samples we have measured. The straight lines represent the linear fit in an accelerating field. (b) A plot of $\ln(I_0/T^2)$ vs. $1/T$ (black dots) and its linear fit line (the red line). Here I_0 is the zero-field current, I_a is the current collected by the anode and U is the anode voltage.

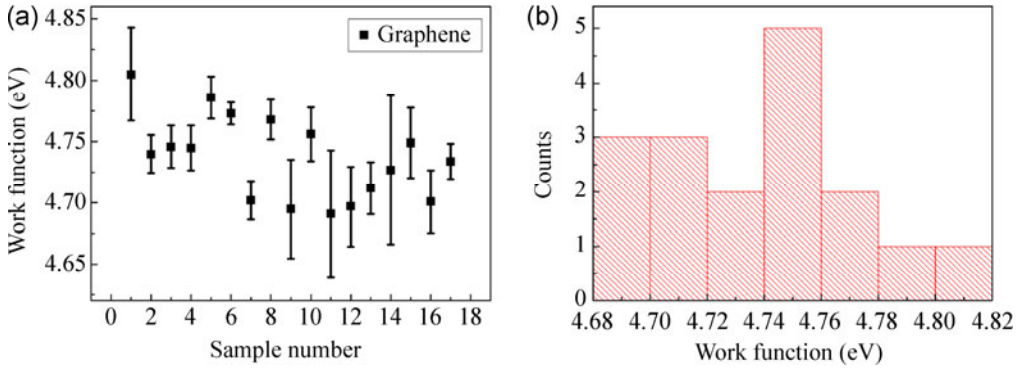

Figure 6 (a) Derived WF of graphene of different samples. (b) Histogram of the measured WF of graphene.

In addition to the SEM images shown in Fig. 2, Raman spectra of graphene before and after annealing also proved its structural integrity. Figure 7 shows the Raman spectra of pure CNT films, and CGF before annealing and after annealing. As shown in Table 1, the spectra of CGF before and after annealing both show much higher 2D/G peak height ratios and lower D/G ratios than pure CNT films. This indicates the presence and integrity of graphene on CGF both before and after annealing [29]. Since graphene is ultrathin and optically transparent, the CNT under the graphene will influence the Raman spectra of graphene, resulting in the reduction of the 2D/G ratio of CGF to lower than 4:1 (the typical characteristic value for monolayer graphene [29]). After annealing, the 2D/G ratio is slightly decreased and the D/G ratio is slightly increased. This possibly originates from the small cracks which appear after annealing.

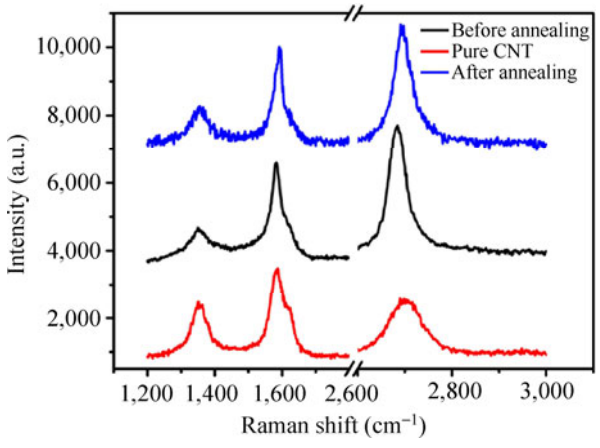

Figure 7 Raman spectra of pure CNT films as well as the CGF before and after annealing at a temperature of 1,800 K for 4 hours. The excitation laser is 514 nm and the spectra are normalized by the intensities of the G peaks.

Table 1 The 2D/G and D/G ratios in the Raman spectra of pure CNT films, CGF before annealing and CGF after annealing

Raman peak ratio	CGF before annealing	CGF after annealing	Pure CNT film
2D/G	1.52	1.31	0.68
D/G	0.31	0.37	0.61

One concern about the graphene on CNT film is whether it retains its intrinsic electronic properties. An important factor that will influence the electronic properties is substrate-induced doping. Due to the porous nature of the CNT substrate, its interaction with graphene is weak. Furthermore, the band structure of CNT means that its Fermi level is almost the same as that of graphene. Hence the doping level of graphene on CGF should be low. Experimentally, the doping level will influence the position of the Raman G and 2D peaks [44]. The position of the Raman G peak of the CGF is 1,583.7 cm^{-1}, and that of the 2D peak is 2,684.7cm^{-1}, which are very close to the values for the undoped state [44]. Another factor that will modify the WF of graphene is the strain [45]. According to theoretical and experimental studies of the CTE of graphene and CNT [35–38], it is estimated that the strain in graphene on CGF is no more than 1.5% during the heating process to 1,800 K (see the ESM for details of the estimation). The concomitant change in WF should be less than 0.1 eV [45], which is within the error range of our measurements. Though the 1.5% strain does not significantly alter the WF, it is sufficient to tear up the polycrystalline graphene along the grain boundaries, as has been demonstrated by strain tests of polycrystalline graphene in previous papers [26, 46, 47].

4 Conclusion

By transferring CVD-grown graphene to a crossed CNT film, we have measured the WF of graphene by the thermionic emission method. The measured WF of graphene ranges from 4.7 to 4.8 eV with the average value being 4.74 eV ± 0.04 eV. The weak interaction due to the porous nature of the CNT film substrate and the adsorbent-free measurement conditions mean that the measured WF of graphene should be close to its intrinsic value. In addition, we also demonstrate that the large area polycrystalline graphene still exhibits an amazing thermal stability after annealing at 1,800 K for more than 4 hours. This suggests it may be used as a replacement for conventional thermionic cathodes.

Acknowledgment

The authors thank Prof. Shuyun Zhou for valuable discussions. The work is financially supported by the National Basic Research Program of China (No. 2012CB932301) and the National Natural Science Foundation of China (Nos. 11274190, 51102144, 51102147, and 90921012).

Electronic Supplementary Material: Supplementary material is available in the online version of this article at http://dx.doi.org/10.1007/s12274-014-0423-1.

References

[1] Bolotin, K. I.; Sikes, K. J.; Jiang, Z.; Klima, M.; Fudenberg, G.; Hone, J.; Kim, P.; Stormer, H. L. Ultrahigh electron mobility in suspended graphene. *Solid State Commun.* **2008**, *146*, 351–355.

[2] Du, X.; Skachko, I.; Barker, A.; Andrei, E. Y. Approaching ballistic transport in suspended graphene. *Nat. Nanotechnol.* **2008**, *3*, 491–495.

[3] Balandin, A. A.; Ghosh, S.; Bao, W.; Calizo, I.; Teweldebrhan, D.; Miao, F.; Lau, C. N. Superior thermal conductivity of single-layer graphene. *Nano Lett.* **2008**, *8*, 902–907.

[4] Ghosh, S.; Calizo, I.; Teweldebrhan, D.; Pokatilov, E. P.; Nika, D. L.; Balandin, A. A.; Bao, W.; Miao, F.; Lau, C. N. Extremely high thermal conductivity of graphene: Prospects for thermal management applications in nanoelectronic circuits. *Appl. Phys. Lett.* **2008**, *92*, 151911.

[5] Ghosh, S.; Nika, D. L.; Pokatilov, E. P.; Balandin, A. A. Heat conduction in graphene: Experimental study and theoretical interpretation. *New J. Phys.* **2009**, *11*, 095012.

[6] Geim, A. K.; Novoselov, K. S. The rise of graphene. *Nat. Mater.* **2007**, *6*, 183–191.

[7] Novoselov, K. S.; Geim, A. K.; Morozov, S. V.; Jiang, D.; Katsnelson, M. I.; Grigorieva, I. V.; Dubonos, S. V.; Firsov, A. A. Two-dimensional gas of massless dirac fermions in graphene. *Nature* **2005**, *438*, 197–200.

[8] Xia, F. N.; Farmer, D. B.; Lin, Y.-M.; Avouris, P. Graphene field-effect transistors with high on/off current ratio and large transport band gap at room temperature. *Nano Lett.* **2010**, *10*, 715–718.

[9] Schwierz, F. Graphene transistors. *Nat. Nanotechnol.* **2010**, *5*, 487–496.

[10] Liu, M.; Yin, X.; Ulin-Avila, E.; Geng, B. S.; Zentgraf, T.; Ju, L.; Wang, F.; Zhang, X. A graphene-based broadband optical modulator. *Nature* **2011**, *474*, 64–67.

[11] Bae, S.; Kim, H.; Lee, Y.; Xu, X. F.; Park, J. S.; Zheng, Y.; Balakrishnan, J.; Lei, T.; Kim, H. R.; Song, Y. I.; et al. Roll-to-roll production of 30-inch graphene films for transparent electrodes. *Nat. Nanotechnol.* **2010**, *5*, 574–578.

[12] Zhou, Y. H.; Fuentes-Hernandez, C.; Shim, J.; Meyer, J.; Giordano, A. J.; Li, H.; Winget, P.; Papadopoulos, T.; Cheun, H.; Kim, J.; et al. A universal method to produce low-work function electrodes for organic electronics. *Science* **2012**, *336*, 327–332.

[13] Filleter, T.; Emtsev, K. V.; Seyller, T.; Bennewitz, R. Local work function measurements of epitaxial graphene. *Appl. Phys. Lett.* **2008**, *93*, 133117.

[14] Yu, Y.-J.; Zhao, Y.; Ryu, S.; Brus, L. E.; Kim, K. S.; Kim, P. Tuning the graphene work function by electric field effect. *Nano Lett.* **2009**, *9*, 3430–3434.

[15] Yan, L.; Punckt, C.; Aksay, I. A.; Mertin, W.; Bacher, G. Local voltage drop in a single functionalized graphene sheet characterized by Kelvin probe force microscopy. *Nano Lett.* **2011**, *11*, 3543–3549.

[16] Wang, B.; Caffio, M.; Bromley, C.; Früchtl, H.; Schaub, R. Coupling epitaxy, chemical bonding, and work function at the local scale in transition metal-supported graphene. *ACS Nano* **2010**, *4*, 5773–5782.

[17] Murata, Y.; Starodub, E.; Kappes, B. B.; Ciobanu, C. V.; Bartelt, N. C.; McCarty, K. F.; Kodambaka, S. Orientation-dependent work function of graphene on Pd(111). *Appl. Phys. Lett.* **2010**, *97*, 143114.

[18] Siokou, A.; Ravani, F.; Karakalos, S.; Frank, O.; Kalbac, M.; Galiotis, C. Surface refinement and electronic properties of graphene layers grown on copper substrate: An XPS, UPS and EELS study. *Appl. Surf. Sci.* **2011**, *257*, 9785–9790.

[19] Takahashi, T.; Tokailin, H.; Sagawa, T. Angle-resolved ultraviolet photoelectron spectroscopy of the unoccupied band structure of graphite. *Phys. Rev. B* **1985**, *32*, 8317–8324.

[20] Oshim, C.; Nagashima, A. Ultra-thin epitaxial films of graphite and hexagonal boron nitride on solid surfaces. *J. Phys. Condens. Matter* **1997**, *9*, 1–20.

[21] Chan, K. T.; Neaton, J. B.; Cohen, M. L. First-principles study of metal adatom adsorption on graphene. *Phys. Rev. B* **2008**, *77*, 235430.

[22] Hicks, J.; Shepperd, K.; Wang, F.; Conrad, E. H. The structure of graphene grown on the SiC (000$\bar{1}$) surface. *J. Phys. D. Appl. Phys.* **2012**, *45*, 154002.

[23] Hicks, J.; Conrad, E. H. Graphene investigated by synchrotron radiation. *MRS Bull.* **2012**, *37*, 1203–1213.

[24] Riedl, C.; Coletti, C.; Starke, U. Structural and electronic properties of epitaxial graphene on SiC(0 0 0 1): A review of growth, characterization, transfer doping and hydrogen intercalation. *J. Phys. D. Appl. Phys.* **2010**, *43*, 374009.

[25] Ramprasad, R.; von Allmen, P.; Fonseca, L. R. C. Contributions to the work function: A density-functional study of adsorbates at graphene ribbon edges. *Phys. Rev. B* **1999**, *60*, 6023–6027.

[26] Lin, X. Y.; Liu, P.; Wei, Y.; Li, Q. Q.; Wang, J. P.; Wu, Y.; Feng, C.; Zhang, L. N.; Fan, S. S.; Jiang, K. L. Development of an ultra-thin film comprised of a graphene membrane and carbon nanotube vein support. *Nat. Commun.* **2013**, *4*, 2920.

[27] Wei, Y.; Jiang, K. L.; Feng, X. F.; Liu, P.; Liu, L.; Fan, S. S. Comparative studies of multiwalled carbon nanotube sheets before and after shrinking. *Phys. Rev. B* **2007**, *76*, 045423.

[28] Li, X. S.; Cai, W. W.; An, J.; Kim, S.; Nah, J.; Yang, D.; Piner, R.; Velamakanni, A.; Jung, I.; Tutuc, E.; et al. Large-area synthesis of high-quality and uniform graphene films on copper foils. *Science* **2009**, *324*, 1312–1314.

[29] Ferrari, A. C.; Meyer, J. C.; Scardaci, V.; Casiraghi, C.; Lazzeri, M.; Mauri, F.; Piscanec, S.; Jiang, D.; Novoselov, K. S.; Roth, S.; et al. Raman spectrum of graphene and graphene layers. *Phys. Rev. Lett.* **2006**, *97*, 187401.

[30] Jiang, K. L.; Li, Q. Q.; Fan, S. S. Spinning continuous carbon nanotube yarns. *Nature* **2002**, *419*, 801.

[31] Xiao, L.; Chen, Z.; Feng, C.; Liu, L.; Bai, Z.-Q.; Wang, Y.; Qian, L.; Zhang, Y. Y.; Li, Q. Q.; Jiang, K. L.; et al. Flexible, stretchable, transparent carbon nanotube thin film loudspeakers. *Nano Lett.* **2008**, *8*, 4539–4545.

[32] Liu, P.; Wei, Y.; Jiang, K. L.; Sun, Q.; Zhang, X. B.; Fan, S. S.; Zhang, S. F.; Ning, C. G.; Deng, J. K. Thermionic emission and work function of multiwalled carbon nanotube yarns. *Phys. Rev. B* **2006**, *73*, 235412.

[33] Lee, Y.; Bae, S.; Jang, H.; Jang, S.; Zhu, S.-E.; Sim, S. H.; Song, Y. I.; Hong, B. H.; Ahn, J.-H. Wafer-scale synthesis and transfer of graphene films. *Nano Lett.* **2010**, *10*, 490–493.

[34] Li, X. S.; Zhu, Y. W.; Cai, W. W.; Borysiak, M.; Han, B. Y.; Chen, D.; Piner, R. D.; Colombo, L.; Ruoff, R. S. Transfer of large-area graphene films for high-performance transparent conductive electrodes. *Nano Lett.* **2009**, *9*, 4359–4363.

[35] Li, C. Y.; Chou, T.-W. Axial and radial thermal expansions of single-walled carbon nanotubes. *Phys. Rev. B* **2005**, *71*, 235414.

[36] Yoon, D.; Son, Y.-W.; Cheong, H. Negative thermal expansion coefficient of graphene measured by raman spectroscopy. *Nano Lett.* **2011**, *11*, 3227–3231.

[37] Jiang, H.; Hwang, K. C.; Liu, B.; Huang, Y. Thermal expansion of single wall carbon nanotubes. *J. Eng. Mater-Trans. ASME* **2004**, *126*, 265–270.

[38] Jiang, J.-W.; Wang, J.-S.; Li, B. W. Thermal expansion in single-walled carbon nanotubes and graphene: Nonequilibrium green's function approach. *Phys. Rev. B* **2009**, *80*, 205429.

[39] Singh, V.; Sengupta, S.; Solanki, H. S.; Dhall, R.; Allain, A.; Dhara, S.; Pant, P.; Deshmukh, M. M. Probing thermal expansion of graphene and modal dispersion at low-temperature using graphene nanoelectromechanical systems resonators. *Nanotechnology* **2010**, *21*, 165204.

[40] Reimann, A. L. *Thermionic Emission*. Chapman & Hall, Ltd.: London, 1934.

[41] Richardson, O. W. *The Emission of Electricity from Hot Bodies*. Longmans, Green and Co.: London, New York etc., 1921.

[42] Liu, P.; Sun, Q.; Zhu, F.; Liu, K.; Jiang, K. L.; Liu, L.; Li, Q. Q.; Fan, S. S. Measuring the work function of carbon nanotubes with thermionic method. *Nano Lett.* **2008**, *8*, 647–651.

[43] Taylor, B. N.; Kuyatt, C. E. Guidelines for evaluating and expressing the uncertainty of NIST measurement results. *NIST Techenical Note 1297, 1994 Edition*. http://physics.nist.gov/Pubs/guidelines/TN1297/tn1297s.pdf. (Accessed on November 3, 2013)

[44] Das, A.; Pisana, S.; Chakraborty, B.; Piscanec, S.; Saha, S. K.; Waghmare, U. V.; Novoselov, K. S.; Krishnamurthy, H. R.; Geim, A. K.; Ferrari, A. C.; et al. Monitoring dopants by raman scattering in an electrochemically top-gated graphene transistor. *Nat. Nanotechnol.* **2008**, *3*, 210–215.

[45] Choi, S. M.; Jhi, S. H.; Son, Y. W. Effects of strain on electronic properties of graphene. *Phys. Rev. B* **2010**, *81*, 081407.

[46] Sun, J. K.; Li, Y. H.; Peng, Q. Y.; Hou, S. C.; Zou, D. C.; Shang, Y. Y.; Li, Y. B.; Li, P. X.; Du, Q. J.; Wang, Z. H.; et al. Macroscopic, flexible, high-performance graphene ribbons. *ACS Nano* **2013**, *7*, 10225–10232.

[47] Lin, Q.-Y.; Jing, G. Y.; Zhou, Y.-B.; Wang, Y.-F.; Meng, J.; Bie, Y.-Q.; Yu, D.-P.; Liao, Z.-M. Stretch-induced stiffness enhancement of graphene grown by chemical vapor deposition. *ACS Nano* **2013**, *7*, 1171–1177.